UC Riverside
Previously Published Works

Title
Comprehensive Simultaneous Shipboard and Airborne Characterization of Exhaust from a Modern Container Ship at Sea

Authors
Murphy, Shane M
Agrawal, Harshit
Sorooshian, Armin
et al.

Peer reviewed

Research

Comprehensive Simultaneous Shipboard and Airborne Characterization of Exhaust from a Modern Container Ship at Sea

SHANE M. MURPHY,[†]
HARSHIT AGRAWAL,[‡,§]
ARMIN SOROOSHIAN,[†] LUZ T. PADRÓ,[∥]
HARMONY GATES,[†] SCOTT HERSEY,[†]
W. A. WELCH,[§] H. JUNG,[§,∥] J. W. MILLER,[‡,§]
DAVID R. COCKER III,[‡,§]
ATHANASIOS NENES,[⊥,#]
HAFLIDI H. JONSSON,[▽] RICHARD C. FLAGAN,[†]
AND JOHN H. SEINFELD[†,*]

Departments of Environmental Science and Engineering and Chemical Engineering, California Institute of Technology, Pasadena, California 91125, Departments of Chemical, Environmental, and Mechanical Engineering, University of California, Riverside, California 92521, College of Engineering-Center for Environmental Research and Technology, 1084 Columbia Avenue, Riverside, California 92507, School of Chemical and Biomolecular Engineering, School of Earth and Atmospheric Sciences, and School of Mechanical Engineering, Georgia Institute of Technology, Atlanta, Georgia 30332, and Center for Interdisciplinary Remotely-Piloted Aircraft Studies, Naval Postgraduate School, Monterey, California 93933

We report the first joint shipboard and airborne study focused on the chemical composition and water-uptake behavior of particulate ship emissions. The study focuses on emissions from the main propulsion engine of a Post-Panamax class container ship cruising off the central coast of California and burning heavy fuel oil. Shipboard sampling included micro-orifice uniform deposit impactors (MOUDI) with subsequent off-line analysis, whereas airborne measurements involved a number of real-time analyzers to characterize the plume aerosol, aged from a few seconds to over an hour. The mass ratio of particulate organic carbon to sulfate at the base of the ship stack was 0.23 ± 0.03, and increased to 0.30 ± 0.01 in the airborne exhaust plume, with the additional organic mass in the airborne plume being concentrated largely in particles below 100 nm in diameter. The organic to sulfate mass ratio in the exhaust aerosol remained constant during the first hour of plume dilution into the marine boundary layer. The mass spectrum of the organic fraction of the exhaust aerosol strongly resembles that of emissions from other diesel sources and appears to be predominantly hydrocarbon-like organic (HOA) material. Background aerosol which, based on air mass back trajectories, probably consisted of aged ship emissions and marine aerosol, contained a lower organic mass fraction than the fresh plume and had a much more oxidized organic component. A volume-weighted mixing rule is able to accurately predict hygroscopic growth factors in the background aerosol but measured and calculated growth factors do not agree for aerosols in the ship exhaust plume. Calculated CCN concentrations, at supersaturations ranging from 0.1 to 0.33%, agree well with measurements in the ship-exhaust plume. Using size-resolved chemical composition instead of bulk submicrometer composition has little effect on the predicted CCN concentrations because the cutoff diameter for CCN activation is larger than the diameter where the mass fraction of organic aerosol begins to increase significantly. The particle number emission factor estimated from this study is 1.3×10^{16} (kg fuel)$^{-1}$, with less than $^1/_{10}$ of the particles having diameters above 100 nm; 24% of particles (>10 nm in diameter) activate into cloud droplets at 0.3% supersaturation.

* Corresponding author e-mail: seinfeld@caltech.edu.
[†] California Institute of Technology.
[‡] Department of Chemical and Environmental Engineering, University of California, Riverside.
[§] Center for Environmental Research and Technology, University of California, Riverside.
[∥] Department of Mechanical Engineering, University of California, Riverside.
[⊥] School of Chemical and Biomolecular Engineering, Georgia Institute of Technology.
[#] School of Earth and Atmospheric Sciences, Georgia Institute of Technology.
[▽] Center for Interdisciplinary Remotely-Piloted Aircraft Studies, Naval Postgraduate School.

1. Introduction

Ship exhaust is estimated to represent an appreciable fraction of global NO$_x$ (21 Tg y^{-1}), SO$_x$ (12 Tg y^{-1}), and hydrocarbon emissions (1.96 Tg y^{-1}) (*1*). Ship emissions are also thought to be a significant contributor to global particulate mass (PM, 1.67 Tg y^{-1}), though emission factors for PM remain highly uncertain (*1−3*). Particles emitted from ships impact climate through both direct and indirect effects and are often emitted close to populated coastlines where they impact air quality (*2, 4, 5*). In their 2003 study on the global impact of ship emissions, Corbett and Koehler (*6*) state that error in the estimated fuel consumption of the world fleet (based on estimates of the number, type, and activity level of vessels in different regions of the world) is the most important uncertainty for every type of ship emission except PM, for which the emission factor itself remains the dominant uncertainty. Relatively little data exist concerning the composition of particles emitted from ships and the ability of those particles to grow by hygroscopic water uptake and act as cloud condensation nuclei (*1, 3, 7*). While it has been established that fresh particulate emissions from ships consist of sulfuric acid, organics, and soot, estimates of the organic mass fraction vary widely (*8−10*). Undoubtedly, much of the variation in the particulate composition stems from the type of fuel used, but because heavy fuel oil (HFO) represents over 80% of the fuel consumed by the world fleet, emissions from HFO clearly need to be characterized. Another source of variation in particulate emissions is ship type, though the majority of worldwide emissions are from large cargo or container vessels (*6*). Finally, engine type and load can significantly influence both particle number and composition, though the amount of time ships spend entering and exiting port with highly varying engine loads is a relatively small fraction of overall operating time.

Emission studies conducted on engine test beds offer obvious advantages in that engine load can be controlled,

TABLE 1. Selected Heavy Fuel Oil Properties

product grade	IFO 380
density at 15 °c	988.5 kg/m^3
viscosity at 50 °c	290.6 mm^2/s
sulfur	3.01% m/m
ash	0.05% m/m
vanadium	75 mg/kg
nickel	29 mg/kg

fuel characteristics are precisely known, and testing can be conducted in a stationary, stable environment (8, 11). While these test-bed studies provide important insight into the emission characteristics of different engines at various loads, they need to be evaluated against measured emissions from engines in actual usage at sea. To determine the relationship between test-bed results and in situ emissions, groups have begun to measure emissions inside the stacks of vessels under sail (12, 13). Other groups have used airborne platforms to characterize particulate ship emissions in the marine atmosphere (3, 7, 11). However, when there is limited knowledge of the fuel being used or the operating conditions of the vessel, it is difficult to relate airborne emissions measurements to fuel consumption inventories. Corbett (14) summarized the gap in the current literature as follows, "By directly measuring what the engine emits at the stack with pollution chemistry "seen by the environment" in the aging plume, we may improve large-scale inventories used in chemical transport models."

We report here the first study with simultaneous in-stack and airborne measurements of emissions from a container ship. Shipboard measurements give detailed gas and particle-phase emissions for a wide range of chemical species, while airborne measurements are focused on particulate number, mass, composition, hygroscopic growth, and CCN activity. We evaluate the relationship between shipboard and airborne measurements and explore how these findings impact the characterization of emissions from this important class of ships.

2. Materials and Methods

2.1. Container Ship. The ship, representative of a modern Post-Panamax class container ship (Panamax = maximum size allowed through the Panama Canal), was 347 m long, with a gross tonnage (GT) of 91 690 and a capacity of 8680 TEUs (20-foot equivalent unit). The main propulsion engine (ME) of the vessel was a 2-stroke, slow-speed diesel engine (12k90MC, build: Hitachi MAN B&W 12K90Mk mk 6 (1998)). The engine's rated power and speed are 54840 kW and 94 r/min with a maximum pressure at maximum continuous rating (MCR) of 141 bar. During the study, load was stable with ME running at 57% of maximum power, approximately 31.2 MW, and 81 rpm. The ME operated on heavy fuel oil (HFO); selected properties are in Table 1, and the ME exhaust included a heat recovery section after the on-board sampling section.

2.2. Shipboard Platform Measurements. A detailed description of the shipboard methods for sampling and analysis of gases and particulate matter (PM) is given in Section S1 of the Supporting Information (SI) and briefly described here. In-stack measurements conformed to the requirements of ISO 8178-1 (15). The sampling approach for PM and speciated hydrocarbons involved the use of a partial flow dilution system with single venturi and is shown in SI Figure S1 and described in Agrawal et al. (13). While ISO 8178-1 allows a transfer line of 5 m, no transfer line was used in this study based on previous experience showing significant loss of particulate mass in the transfer line. Concentrations of CO_2 and NO_x were measured in both the raw exhaust

gas and dilution tunnel using the exhaust gas analyzer (EGA). The dilution ratio in the dilution tunnel, determined from either CO_2 or NO_x concentrations, agreed within 5%, as specified in the reference method (15).

Emission measurement of different gases, PM$_{2.5}$ (particulate matter of diameter <2.5 μm) mass, size resolved PM composition, metals, ions, elemental and organic carbon, selected hydrocarbon species, including polycyclic aromatic hydrocarbons (PAHs), carbonyls, and n-alkanes, were performed off-line following standard methods (15−19). The SO_2 data are calculated from the sulfur level in the fuel as per ISO 8178-1 (15). Other PM measurements were made with: a MOUDI, a thermophoretic sampler with transmission electron micrcoscopy (TEM) grids (model 3320C-CF, SPI Inc.), and Dekati Mass Monitor (20). TEM grids were analyzed for nonorganic elemental composition using EDS (energy dispersive X-ray spectroscopy).

2.3. Aircraft-Based Measurements. The Center for Interdisciplinary Remotely Piloted Aircraft Studies (CIRPAS) Twin Otter aircraft performed a series of passes through the exhaust plume of the container ship on July 16, 2007. The ship−plane rendezvous occurred in the Pacific Ocean 65 km west of the central California Coast at 122° west longitude and 35° north latitude. The Twin Otter remained in the vicinity of the ship for roughly 2.5 h, characterizing the aerosol properties within the plume and background air. Plume aerosol was measured at ages ranging from a few seconds to over an hour.

2.3.1. Aerosol Number and Volume. Aerosol number concentrations were measured by three independent condensation particle counters (CPCs), two TSI model 3010 counters with a minimum detection diameter of 10 nm and a saturation threshold of 10^4 particles cm^{-3} and one ultrafine condensation particle counter (TSI model 3025) with a minimum detection diameter of 3 nm and a saturation threshold of 10^6 particles cm^{-3}. In the concentrated exhaust plume just behind the ship, all three CPC's were saturated; when this occurred, number concentration data were obtained from the differential mobility analyzer (DMA) (D_m = 10−800 nm) which is not subject to saturation until much higher concentrations because it classifies the aerosol before optical counting. However, the time resolution of the DMA is much slower (74 s) than the CPCs (1 s).

Aerosol volume was determined by the DMA and an external passive cavity aerosol spectrometer probe (0.1−3 μm) (PCASP, PMS Inc., modified by DMT Inc.). The response of the PCASP probe to different diameter particles was calibrated using polystyrene latex spheres (refractive index = 1.58) and this calibration was used for all data analysis. While the PCASP cannot measure particles below 100 nm, it offers the advantage of 1 s time resolution. The PCASP nominally operates at ambient relative humidity while during this flight, because of problems with the Nafion drier, the DMA was operated at relative humidities between 40 and 50%.

2.3.2. Aerosol Mass, Chemistry, and Absorption. Submicrometer aerosol mass and size-resolved chemical composition were measured by an Aerodyne compact time of flight aerosol mass spectrometer (C-ToF-AMS). Submicron water-soluble ions were measured by a particle into liquid sampler - ion chromatograph (PILS-IC, Brechtel Mfg. Inc.). Aerosol optical absorption was measured by a three-wavelength particle soot absorption photometer (PSAP, Radiance Research).

Details concerning the C-ToF-AMS can be found in Drewnick et al. (21). For this airborne deployment the C-ToF-AMS was fitted with a pressure-controlled inlet (22), a 3.5% chopper, the vaporizer was operated at 550 °C, and ion extraction occurred at a rate of ~60 kHz. Detection limits for the instrument, calculated as three times the standard

deviation of the noise for filtered air, are <0.05 $\mu g\ m^{-3}$ for all species measured, though, in practice, detection is limited by counting statistics at low aerosol loadings. One important issue concerning C-ToF-AMS data is the collection efficiency of particles within the instrument (23). In this study, all C-ToF-AMS mass loadings were multiplied by a factor of 2 (collection efficiency = 0.5) to attain agreement between the sulfate measurements of the C-ToF-AMS and the PILS-IC during periods where there were no rapid fluctuations in particulate mass loading. A collection efficiency of 0.5 has been observed in numerous other field studies with the AMS (24) and in this study it gives excellent agreement with both the PILS sulfate measurement and DMA derived mass loadings, as described in Section 3.3.

The PILS-IC is described in Sorooshian et al. (25) with specifics related to airborne operation given in Sorooshian et al. (26). For this study, instrument uncertainty was established as ±7%. Collected aerosol in solution was delivered to a rotating carousel containing 72 vials, each of which contains material representing a period of ~5 min of flight, or alternatively, a distance of 15 km in flight (aircraft speed ~50 m/s).

The design of the three wavelength PSAP used in this study is described in Virkkula et al. (27). The PSAP measures cumulative light absorption at 467, 530, and 660 nm as particles are collected onto a filter. All absorption measurements presented in this paper have been corrected for scatter using the methods described in Virkkula et al. (27).

2.3.3. Aerosol Hygroscopic Growth and Cloud Condensation Nuclei Activity. Subsaturated aerosol water uptake was measured by a recently developed instrument, the differential aerosol sizing and hygroscopicity spectrometer probe (DASH-SP; Brechtel Mfg Inc.) while activation of cloud condensation nuclei (CCN) was measured by a flow thermal gradient cloud condensation nuclei counter (CCNc, Droplet Measurement Technologies Inc.) The DASH-SP is described in detail in Sorooshian et al. (28). During this study, the DASH-SP provided simultaneous measurements of growth factor at different relative humidities (RH) for dry DMA-selected particle diameters between D_m = 150−200 nm; the time resolution for this size range inside and outside of the plume was 1−10 s and 10−30 s, respectively. One humidifier was operated dry (RH < 8%), and the other three were at RH settings of 74, 85, and 92%. The uncertainty associated with growth factor measurements is ±4.5%, and the uncertainty in the RH measurement is ±1.5%. The CCNc is described in detail in Roberts and Nenes (29) and Lance et al. (30). For this study, the instrument was operated at supersaturations between 0.1 and 0.4%.

2.4. Theory for Predicting Subsaturated Hygroscopic Growth. Owing to its simplicity and frequent application, an assumption of independent and additive water uptake by each individual chemical component of a particle was used to predict hygroscopic growth in this study with composition measurements obtained from the C-ToF-AMS (31, 32):

$$GF_{mixed}(a_w) = \left(\sum_i \varepsilon_i GF_i(a_w)^3\right)^{\frac{1}{3}} \tag{1}$$

where GF_{mixed} is the hygroscopic growth factor of the mixed particle, GF_i is the hygroscopic growth factor of pure compound i, a_w is the activity coefficient of water, and ϵ_i is the volume fraction of pure compound i in the dry particle. In applying eq 1 we set a_w = RH (33). Growth factors for the pure inorganic components were obtained from the aerosol inorganics model (34, 35). In the DASH-SP, particles are processed at an RH very near zero before being rehumidified. Since ammonium sulfate does not deliquesce until 79% (33), it is assigned a growth factor of unity at 74% RH. Because C-ToF-AMS results indicate a hydrocarbon-like and presum-

ably hydrophobic organic aerosol component in the ship-exhaust plume, the growth factor for organic material is assumed to be unity at all RH settings.

2.5. Theory for Cloud Condensation Nuclei (CCN) Closure. "CCN closure", that is, comparison of CCN predictions based on knowledge of particle size and composition with direct measurements of CCN concentrations, is an evaluation of the extent to which CCN behavior can be predicted theoretically using Köhler theory (36). CCN closure calculations within the exhaust plume of the ship were performed at supersaturations ranging from 0.1 to 0.33%. Because the DMA was operated at relative humidities ranging from 40 to 50% during the study, measured aerosol particles contained significant amounts of water, especially in the ship plume where sulfuric acid was the most abundant species. Because prediction of CCN concentrations requires knowledge of the dry size and composition of particles, an algorithm was developed to calculate dry size distributions from the measured humid distributions. First, size-resolved C-ToF-AMS data (averaged over the 74 s scan time of the DMA) were shifted in diameter space until they aligned with the volume distribution from the DMA. Once the mass and volume distributions were aligned, the nonrefractory particle composition of each DMA diameter bin was determined from the C-ToF-AMS data (see Section 3.3 for a discussion of why the dry composition from the C-ToF-AMS, measured versus vacuum aerodynamic diameter, can be aligned with the humid volume distribution from the DMA, measured versus electrical mobility diameter). Next, with knowledge of the composition of each DMA diameter bin, the ISORROPIA program (37) was used to determine the amount of water that the particles in each diameter bin contain at thermodynamic equilibrium at the operating relative humidity of the DMA. Finally the particle volume without water was calculated (assuming volume additivity), particles were rebinned into new smaller size bins, and the average composition of the new diameter bins was calculated. Following this procedure, particle diameters within the ship exhaust plume were found to be between 15 and 28% smaller when dry than when measured by the DMA at ~45% RH. The percentage decrease in diameter was almost exclusively determined by the mass fraction of organic (assumed insoluble) present in a given DMA diameter bin. Data from the CCNc were also averaged to match the time resolution of the scanning DMA meaning one closure calculation can be performed every 74 s except when the CCNc instrument is switching between supersaturations.

Based on C-ToF-AMS and DASH-SP results to be discussed, the aerosol was treated as an internal mixture when predicting CCN concentrations. Because the C-ToF-AMS cannot measure refractory material, black carbon and ash are assumed to be negligible in this closure study (impacts of this assumption are discussed in Section 4.4). Two chemical composition scenarios were considered in the closure: (a) bulk composition, which assumes all particles have the same composition and (b) size-resolved composition, which assigns a specific composition to each particle size. In each of these compositional scenarios, the measured sulfate molar ratio, SR = $[NH_4^+]/[SO_4^{2-}]$, was used to estimate the composition of the inorganic fraction. When SR ≤ 1, the sulfate is assumed to be a mixture of NH_4HSO_4 and H_2SO_4, when 1 < SR < 2, the sulfate is assumed to be a mixture of NH_4HSO_4 and $(NH_4)_2SO_4$, and when SR ≥ 2, the sulfate is considered to be solely $(NH_4)_2SO_4$. In the exhaust plume, the sulfate fraction consisted mainly of H_2SO_4. Because ammonium levels were very low in the ship-exhaust plume (SR ~ 0.1) the size-resolved ammonium measurements from the C-ToF-AMS were too noisy to be used in CCN closure calculations. Instead, the mass ratio of ammonium to sulfate from the bulk composition was assumed at all sizes. Particles

FIGURE 1. Photograph taken of the container ship from the cabin of the CIRPAS Twin Otter (the plane's wing tip is in the foreground) during the study. The exhaust plume is visible traveling with the mean wind at ~10° angle to the heading of the ship, which can be inferred by the visible wake.

were assumed to have the surface tension of water and organics were treated as insoluble.

The effective van't Hoff factor, ν_s (which includes an estimate of the osmotic coefficient), is assumed to be 2.5 for ammonium sulfate, obtained from Pitzer activity coefficients (*38, 39*) for ammonium sulfate CCN with critical supersaturation between 0.2 and 0.6%. Effective van't Hoff factors for sulfuric acid and ammonium bisulfate are assumed to be 2 and 2.5, respectively (*38–40*). The critical supersaturation, s_c, for each particle with dry diameter d, is calculated from Köhler theory (*33*),

$$s_c = \left[\frac{256}{27}\left(\frac{M_w\sigma}{RT\rho_w}\right)^3\left(\frac{M_S}{\rho_S}\right)\left(\frac{\rho_w}{M_w}\right)\frac{d^3}{\epsilon_S\nu_S}\right]^{1/2} \quad (2)$$

where R is the universal gas constant, T is the ambient temperature, σ is the surface tension of the CCN at the point of activation, M_s is the molar mass of the solute, and M_w and ρ_w are the molar mass and density of water, respectively. The volume fraction of solute, ϵ_s, can be calculated as a function of the mass fraction of solute, m_s, and its density, ρ_s,

$$\epsilon_S = \frac{\dfrac{m_S}{\rho_S}}{\dfrac{m_S}{\rho_S} + \dfrac{1 - m_S}{\rho_i}} \quad (3)$$

where ρ_i is the density of the insoluble organic (assumed to be 1.6 g cm^{-3}, as discussed subsequently). A particle is

counted as a CCN when its calculated s_c is less than or equal to the supersaturation of the CCNc. Predicted and measured CCN are then compared to assess closure.

3. Results

3.1. Flight Tracks and Meteorology. Figure 1 is a photo taken from the Twin Otter aircraft during the study; the plume was visible to the naked eye for a considerable distance downwind of the ship. There was a steady 10–15 m s^{-1} wind from 311° NW which was blowing at a 10° angle to the ship's path, as can be seen by the different paths of the exhaust plume and ship wake in Figure 1. The flight track for the CIRPAS Twin Otter is shown in Figure 2. Marker size is proportional to sulfate concentration and indicates the relative dilution of the exhaust plume being emitted from the ship. Plume age was estimated from a simple calculation based on the distance between the ship and the aircraft at the time of measurement, knowledge of the ship's velocity (11.3 m s^{-1}) and heading (322° NW), and the average wind speed (11.4 m s^{-1}) and direction (311° NW) during the period between when the exhaust was emitted from the ship and measurement by the aircraft.

The marine boundary layer was well mixed during the 2.5 h period that the Twin Otter probed the ship plume with a temperature of 14.3 ± 0.4 °C (θ = 287.9 ± 0.1) and a relative humidity of 90–98%. Vertical profiles (Figure S2 in the SI) show an abrupt increase in potential temperature and decrease in relative humidity at approximately 200 m, which is assumed to be the top of the marine boundary layer. Three-
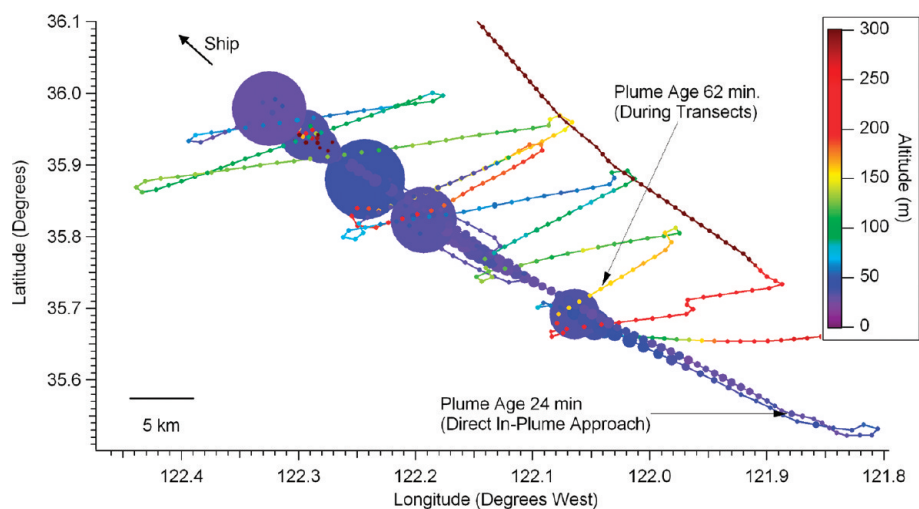
FIGURE 2. Flight track of the CIRPAS Twin Otter during the ship exhaust plume study on July 16, 2007. Marker size is proportional to the mass of sulfate in the particulate phase. The aircraft flew a series of four in-plume approaches to the ship. During the first approach, the estimated exhaust age at the point where the aircraft entered the plume was 24 min. This and each subsequent approach ended when the aircraft reached the stern of the ship, identifiable by the very large sulfate loadings observed there. After finishing the in-plume approaches, a series of 11 downwind transects were flown with the maximum plume age observed during the transects being 62 min. While the location of the 62 min transect may appear closer to the ship than the in-plume observations, it is important to remember that this transect was performed long after the in-plume approaches were finished when the ship had traveled beyond the area shown in the figure.

day Hysplit back trajectories (Figure S3 in the SI) indicate that the air mass present during the study originated in the Pacific Ocean and that there was no direct continental or urban influence on it during the previous 3 days. There is little variation in the back trajectories with altitude, giving further confidence that the measured air was not contaminated by continental outflow (*41*).

Two different flight strategies were used. In the first half of the flight, four direct approaches were made toward the ship, flying in what was estimated to be the center of the plume. Each approach was initiated at a point that was as far from the ship as possible but where the plume was still clearly distinguishable from background aerosol. In these approaches down the ship plume, it was possible to obtain number, volume, and mass distributions and, importantly, to accurately measure the chemical composition of the ship-exhaust aerosol in a region with very high signal-to-noise. Because negligible differences were observed in any of the measured variables between the four direct approaches in the plume, generally we present data only from the first approach, in which the plume was detected at the farthest distance from the ship. The second half of the flight consisted of a number of plume transects made at progressively farther distances from the ship and at altitudes between 30 and 200 m. In this part of the flight the crosswind and vertical structure of the plume and particle aging at longer time scales were examined.

3.2. In-Stack Composition. Table 2 gives emission factors for all of the gas-phase and mixed (gas and particle) phase species measured from the ship's stack. The data represent the average of triplicate measurements made during the period when the aircraft was probing the exhaust plume; the values are similar to those reported by the engine manufacturer on this vessel. In addition to CO_2, NO_x, and SO_2, a wide array of volatile organic compounds were measured, with naphthalene, formaldehyde, acetaldehyde, and acetone being the most abundant.

Table 3 gives the average in-stack emission factors for particulate-phase species. While sulfate is the dominant emission by mass, there is a significant fraction of organic carbon. The cumulative masses of hydrated sulfate, organic carbon, elemental carbon, and estimated ash is about 20% less than the measured particulate mass. The lack of mass

closure is most likely the result of uncertainty in the number of water molecules associated with each sulfate molecule. A ratio of 6.5 H_2O molecules to a H_2SO_4 molecule was used because it represents the lowest energy state for a sulfate–water complex (*12, 13*). Another reason for poor mass closure is that the organic carbon (OC) has not been converted to organic mass (OM). While this would improve closure, it may not be justified given that previous filter-based measurements of diesel exhaust, where denuders were used to remove gas-phase organics, have shown an overestimation of OC mass of approximately 30% caused by adsorption of gas-phase organics onto the filter (*42*). Figure 3 shows size-resolved chemical composition measurements of particulate matter within the ship's stack obtained using a micro-orifice uniform deposit impactor (MOUDI, described in Section S1.4 in the SI). The mass ratio of total carbon to hydrated sulfate (H_2SO_4 + 6.5 H_2O) remains relatively constant with size at 0.12 ± 0.02, but the fraction of unknown mass is much higher at small particle sizes (note that there was too little PM present in size bins above 0.32 μm to exceed the detection limit for sulfate measurement and total PM cannot be measured for the smallest size bin as described in Section S1.4 of the SI).

Figure 4 shows a TEM image from the in-stack thermophoretic sampler. Two populations of nanoparticles are observed; one population ranging from 5 to 8 nm and the other ranging from 30 to 100 nm. The 5–8 nm nanoparticles outnumber the larger nanoparticles, a finding that is consistent with airborne measurements with an ultrafine CPC, discussed subsequently, that show significant number of particles between 3 and 10 nm. EDS analysis shows distinctive peaks of sulfur and vanadium from both populations of particles.

3.3. Particle Number, Volume, and Mass in the Airborne Exhaust Plume. Figure 5 shows particle number concentrations during a series of airborne transects made at progressively farther distances from the ship. Data from the three different CPCs and the PCASP are shown. During the first two transects all three CPCs were saturated, consistent with a DMA-measured concentration of 7.8×10^5 particles cm^{-3} near the ship. The relatively low particle number concentrations reported by the PCASP indicate that the vast majority of particles were less than 100 nm in size. On the third transect, the number concentrations recorded by the ultrafine

TABLE 2. Gaseous Stack Emission Factors in g (kWhr)$^{-1}$ by Chemical Class[a]

compound	emissions factor	compound	emissions factor
NO_x (as NO_2)	20.1 ± 0.1	PAHs[c], alkanes cont'd	
CO	0.29 ± 0.01	Tetradecane	(5.55 ± 0.26) × 10^{-4}
CO_2	638 ± 4	hexadecane	(4.00 ± 1.32) × 10^{-4}
Calc.SO_2[d]	11.9 ± 0.1	octadecane	(3.21 ± 1.13) × 10^{-4}
BTEX[b]		nonadecane	(2.00 ± 0.39) × 10^{-4}
1,3 butadiene	(1.3 ± 0.8) × 10^{-4}	fluorene	(2.50 ± 0.74) × 10^{-4}
benzene	(7.0 ± 0.4) × 10^{-4}	phenanthrene	(5.14 ± 2.15) × 10^{-4}
toluene	(4.4 ± 0.9) × 10^{-4}	anthracene	(1.22 ± 0.66) × 10^{-5}
m&p xylene	(3.3 ± 0.5) × 10^{-4}	fluoranthene	(7.48 ± 2.85) × 10^{-5}
ethyl benzene	(1.1 ± 0.3) × 10^{-4}	eicosane	(2.49 ± 0.64) × 10^{-4}
o-xylene	(1.0 ± 0.05) × 10^{-4}	docosane	(6.84 ± 3.63) × 10^{-4}
carbonyls		tetracosane	(9.55 ± 9.06) × 10^{-4}
formaldehyde	(8.32 ± 4.82) × 10^{-3}	hexacosane	(7.82 ± 7.96) × 10^{-4}
acetaldehyde	(5.21 ± 2.06) × 10^{-3}	octacosane	(7.37 ± 6.02) × 10^{-4}
acetone	(3.12 ± 2.15) × 10^{-3}	triacontane	(3.99 ± 2.41) × 10^{-4}
acrolein, propionaldehyde, crotonaldehyde, methyl ethyl ketone, methacrolein, butyraldehyde, benzaldehyde, n-valeraldehyde, m-tolualdehyde, hexaldehyde	<0.53 × 10^{-3}	pyrene	(4.76 ± 1.48) × 10^{-5}
		benz(a)anthracene	(8.19 ± 1.15) × 10^{-6}
		chrysene	(8.89 ± 0.84) × 10^{-6}
		benzo(b)fluoranthene	(6.35 ± 1.17) × 10^{-6}
PAHs[c] and alkanes		benzo(k)fluoranthene	(4.73 ± 0.83) × 10^{-6}
naphthalene	(3.36 ± 1.06) × 10^{-2}	benzo(a)pyrene	(1.62 ± 0.15) × 10^{-5}
acenaphthylene	(2.35 ± 0.53) × 10^{-5}	indeno(1,2,3-cd)pyrene	(4.86 ± 1.04) × 10^{-6}
acenaphthene	(1.16 ± 0.63) × 10^{-4}	dibenzo(a,h)anthracene	(3.64 ± 1.02) × 10^{-6}
dodecane	(2.34 ± 0.19) × 10^{-4}	benzo(ghi)perylene	(2.66 ± 1.02) × 10^{-5}

[a] Emission factors for PAHs and alkanes are for total (gas and particle phase) emissions. [b] BTEX = benzene, toluene, ethylbenzene, and xylenes, [c] PAH = polycyclic aromatic hydrocarbon. [d] SO_2 gas data is calculated from the sulfur level in the fuel as per ISO 8178 (15).

TABLE 3. Particulate Stack Emission Factors

compound	emissions factor (g/kWhr)
particulate mass (PM)[a]	2.62 ± 0.03
sulfate as $H_2SO_4 \cdot 6.5H_2O$	1.87 ± 0.24
sulfate (dry)	0.84 ± 0.11
organic carbon (OC)	0.193 ± 0.004
elemental carbon (EC)	0.007 ± 0.001
ash[b]	0.085

[a] Particulate mass measurements were made after filter equilibration at RH = 40% and T = 25 °C (see Section S1.2 of the SI for details) [b] Ash emission factor estimated from the ash content in the fuel.

TSI 3025 CPC dropped below the instrument saturation level of 10^5 particles cm^{-3}. The particle number concentration in the center of the plume during all of the transects exceeded 10^4 cm^{-3}, a level at which the TSI 3010 data are unreliable (7.4% coincidence at 10^4 particles cm^{-3}). On the edges of the plume transects, the ultrafine TSI 3025 detected much higher loadings of particles than either TSI 3010, indicating the presence of significant numbers of particles between 3 and 10 nm (the cutoff points for the TSI 3025 and 3010 CPCs, respectively). The ultrafine particles persist even at the longest plume age observed of 62 min.

Figure 6 shows time series from the C-ToF-AMS, PILS, PCASP, and DMA during the first in-plume approach to the ship. Background aerosol, at loadings typical for marine air in this region, is observed until the plume is first encountered at 21:32 UTC. Following plume identification, the aircraft flew in the plume toward the ship until reaching it at 21:49. The particle volumes measured by the PCASP were much lower than those of the other instruments, indicating that not only the majority of the particle number distribution, but also the majority of the particulate volume and mass distributions were below a diameter of 100 nm.

In Figure 6 and all subsequent figures, the mass loadings shown for the C-ToF-AMS have been multiplied by a factor of 2 to correct for particle bounce off the instrument's vaporizer (see Section 2.3.2). The maximum sulfate loadings determined by the C-ToF-AMS inside the exhaust plume are significantly higher than those determined by the PILS, presumably the result of the longer, 5 min, averaging time for a PILS measurement. To confirm that the higher loadings observed in the C-ToF-AMS were not caused by an increase in collection efficiency related to the high concentrations of sulfuric acid in the exhaust plume (24), C-ToF-AMS results are compared with measurements from the DMA, which has enhanced time resolution (74 s scans) relative to the PILS. Comparing the volume measured by the DMA to the C-ToF-AMS mass measurement requires an estimate of the aerosol density. The C-ToF-AMS measures particle vacuum aerodynamic diameter (D_{va}) while the DMA measures electrical mobility diameter (D_m) allowing determination of particle density (ρ_p) (43). If one assumes that the aerosol consists of an internal mixture of spherical particles, the relationship between the two diameters is $\rho_p = (D_{va}/D_m)\rho_o$, where ρ_o is unit density (1 g cm^{-3}).

Figure 7 shows the chemically resolved mass distribution of the in-plume aerosol measured by the C-ToF-AMS along with the number and volume distributions from the DMA. While there is a higher fraction of organic matter in the smaller particles, an assumption of internal mixing appears reasonable in determining an average particle density. Based on the diameter offset between the mass distribution (plotted vs D_{va}) and the volume distribution (plotted vs D_m), the average in-plume particle density is calculated to be 1.4 g cm^{-3}.

Because the DMA was run at relative humidities between 40 and 50%, this represents a wet particle density. It may seem inconsistent to use C-ToF-AMS data where particles are essentially dry (a small amount of water is retained by sulfuric acid in the C-ToF-AMS) and DMA data where they
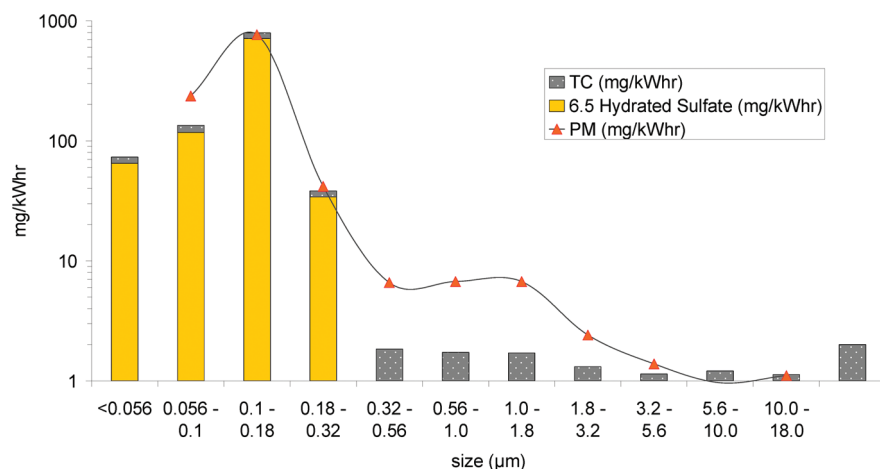
FIGURE 3. Size-resolved particulate chemical composition obtained through the MOUDI/filter setup in the ship's stack. The ratio of total carbon (TC) mass to hydrated sulfur ($H_2SO_4 \cdot 6.5H_2O$) mass remains relatively constant with size (12% <0.056 μm, 14% 0.056–0.1 μm, 9% 0.1–0.18 μm, and 12% 0.18–0.32 μm).
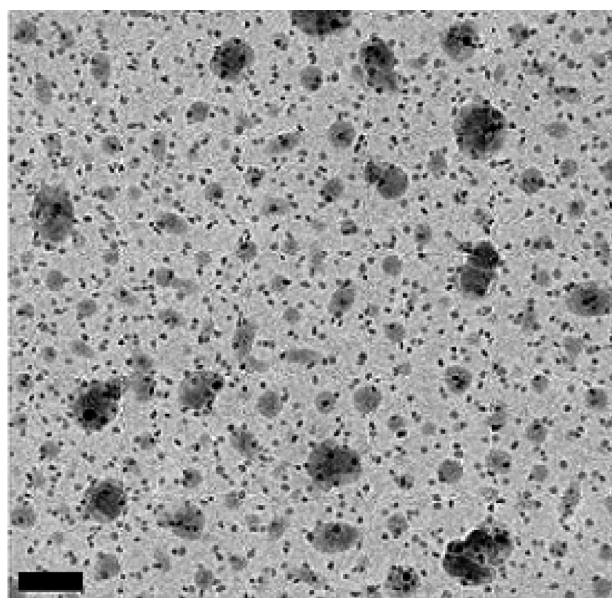

FIGURE 4. TEM image (scale bar in lower left corner = 100 nm) of particles collected with the in-stack thermophoretic sampler. Two classes of particles are observed: (1) nanoparticles in the size range of 5–8 nm and (2) larger particles in a wide size range from 30 to over 100 nm. The nanoparticles outnumber the larger particles. EDS analysis showed distinctive peaks of sulfur and vanadium from both classes of particles.

are wet. However, this is reasonable because of the fortuitous fact that the vacuum aerodynamic diameter of particles composed of sulfuric acid and hydrophobic organic remains virtually unchanged as the particle is dried from 50 to 0% RH. This is because the reduction in size caused by the loss of water is almost exactly compensated for by the increase in density. Using the wet particle density of 1.4 g cm^{-3}, mass loadings can be derived from the DMA volume data. When total particulate mass measured by the C-ToF-AMS is plotted versus the DMA volume multiplied by a wet density of 1.4 g cm^{-3}, the resulting loadings agree within ±10% throughout the plume, except for the point nearest the ship where sufficient time did not exist to complete a full DMA scan. Even at this last point where the highest loading was observed, the two instruments agree to within 20%, with the C-ToF-AMS measuring 470 μg m^{-3} and the DMA, 380 μg m^{-3}. The extent of agreement between the mass measured by the PILS, the C-ToF-AMS, and the DMA-derived mass gives confidence

that none of these instruments was subject to obvious saturation issues and that the collection efficiency of the AMS remained constant throughout the flight.

3.4. Airborne Particulate Composition. Table 4 gives the mass fractions of organic, ammonium, sulfate, and nitrate in the particles directly behind the ship and during successive downwind transects of the exhaust plume. Also given are the contributions of m/z 44 (CO_2^+, higher fractions indicate more oxidation) and 57 ($C_4H_9^+$) higher fraction indicate less oxidation) (44) to the organic mass, the ammonium-to-sulfate molar ratio, and the fraction of the organic mass (measured by the C-ToF-AMS) accounted for by oxalate and other organic acids (measured by the PILS). Organic acid concentrations in the final transect represent primarily background aerosol because the plume transect itself lasted for a few seconds while a PILS vial represents average particle concentrations for a five-minute period. Measurements from the PSAP instrument of aerosol light absorption are an indirect measure of particulate black carbon concentration.

Organics comprise 31% of the aerosol mass immediately aft of the ship. This fraction does not change significantly with age, remaining at 28% after the plume has aged for over an hour. The nonorganic aerosol mass appears to be almost entirely sulfuric acid, given the very low mass fractions of either ammonium or nitrate within the plume. The low mass fraction of organic acids in the plume and the large contribution of m/z 57 relative to m/z 44 indicate that the organic is not well oxidized or readily water soluble (45, 46). The estimated O:C atomic ratio for the plume organic aerosol is 0.20 versus 0.74 for the background aerosol (O:C estimates based on eq 4 and discussed in Section 4.1) (47). Figure 8 shows aerosol mass spectra taken in the fresh ship exhaust, in the exhaust plume after it had aged for 62 min, and in the background marine boundary layer. Also shown in Figure 8 is a reference Aerodyne AMS mass spectrum from the exhaust of a diesel bus (48). While the relative magnitude of the major peaks is slightly different in the diesel bus and ship exhaust particulate mass spectra, the major peaks themselves are the same. These are the same major peaks observed by Phinney et al. (49) during previous observations of particulate ship exhaust with an Aerodyne AMS and they indicate particles composed of saturated and unsaturated hydrocarbons (alkanes, m/z 29, 43, 57, 71, 85,...; alkenes and cycloalkanes, m/z 27, 41, 55, 69, 83,...; dienes, alkynes, and cycloalkenes, m/z 67, 81, 95,...; phenylalkanes, m/z 77, 91, 105, 119,...) (50). Peaks known to be associated with PAHs were also observed in the C-ToF-AMS mass spectrum at m/z values above 200. Also evident in Figure 8 is an increase in
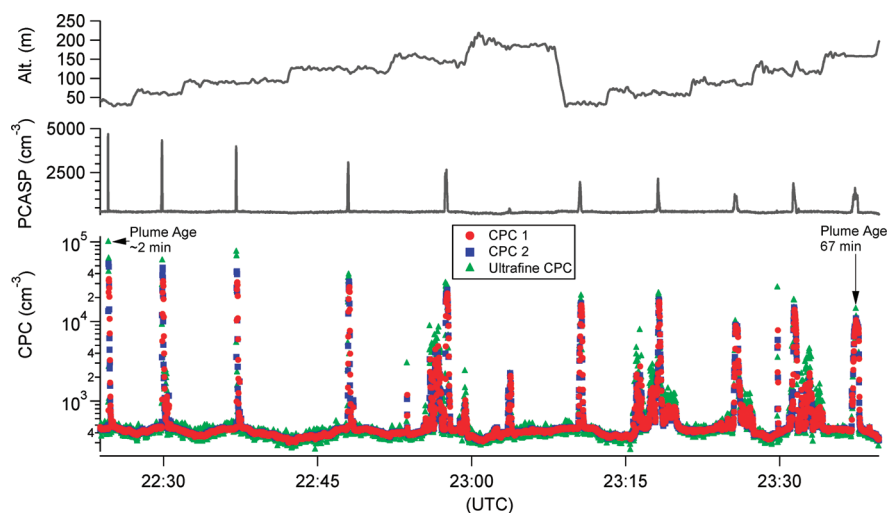
FIGURE 5. Time series of the aerosol number concentration measurements from the TSI 3010 and 3025 CPCs showing significant ultrafine particle concentrations at plume ages up to 1 h. The low PCASP concentrations indicate that the vast majority of particles in the ship exhaust plume are less than 100 nm in diameter. Plume passes were made at several different altitudes.
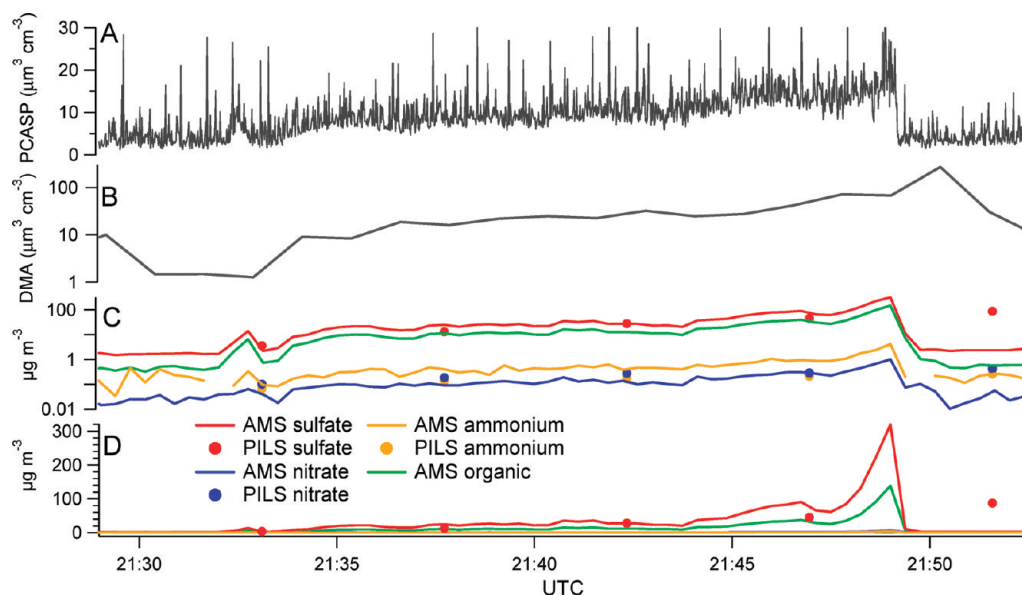

FIGURE 6. Time series of all instruments measuring aerosol mass or volume during the first in-plume approach to the ship. (A) PCASP particle volume (B) DMA particle volume (C and D) AMS and PILS measurements of particle chemistry shown on a log and linear axis, respectively. The plane first enters the exhaust plume at 21:32 UTC, at which point the plume has aged for ~24 min since being emitted from the ship. The plane reaches the stern of the ship at 21:49, though the response of the DMA and the PILS is delayed because of averaging time within the instruments.

the mass fraction of m/z 44 and a decrease in the mass fraction m/z 57 in the more aged spectra, though this is thought to be primarily caused by the influence of the more highly oxidized background aerosol mixing in when the plume dilutes, as will be subsequently discussed.

3.5. Aerosol Hygroscopicity. Figure 9 shows the particle hygroscopic growth factors measured by the DASH-SP and predicted by eq 1 with compositional inputs obtained from the C-ToF-AMS. Average growth factors are given for "in plume", defined as regions where particulate sulfate mass and CN number were more than double those of the background aerosol, and "out of plume", classified as all nonplume measurements made at similar altitudes to the in-plume measurements. The sulfate molar ratio, SR = $[NH_4^+]/[SO_4^{2-}]$, was used to determine the composition of the inorganic fraction. The same scheme (described in Section 2.5) was used to define the relative amounts of sulfuric acid, ammonium bisulfate, and ammonium sulfate in both subsaturated hygroscopic growth and CCN calculations. Pre-

dicted particle growth factors were calculated using bulk composition (the average composition of all submicrometer particles). While the DASH-SP measures particles with mobility diameters between 150 and 200 nm, bulk composition was used because the improvement in signal-to-noise was judged to be more important than the rather negligible difference (typically <5%) between bulk composition and the composition of particles in this size range. Organics were assumed to be hydrophobic and assigned a growth factor of unity when calculating hygroscopic growth factors, both in the ship exhaust plume and in the background air.

Because eq 1 requires volume fractions of individual chemical species in the aerosol and the C-ToF-AMS measures mass fractions, it is necessary to estimate the density of each individual chemical component within the particle. Using the techniques described in Section 3.3, the average particle density (at ~45% RH) was determined to be 1.4 g cm^{-3} in the ship-exhaust plume and 1.55 g cm^{-3} outside of the plume. Given the average particle density, the density of the organic
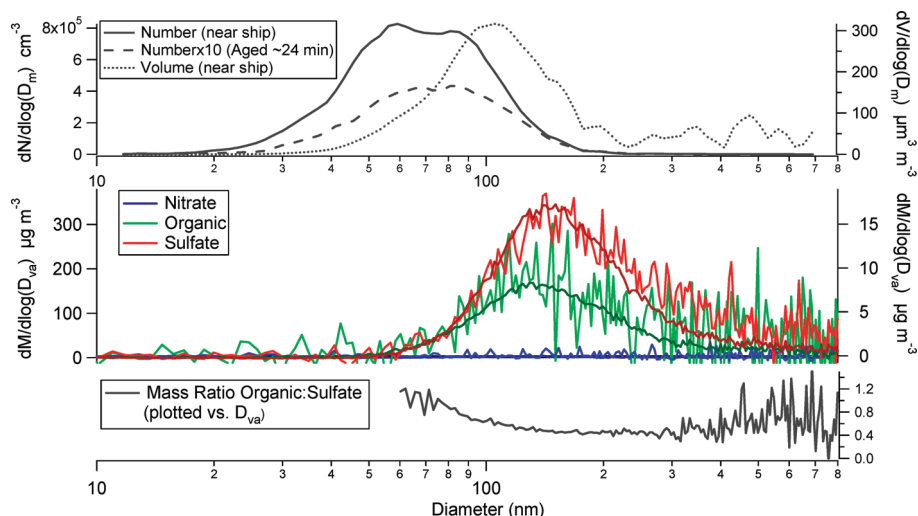
FIGURE 7. Top Panel: Particle number and volume distributions measured by the DMA (at ~45% RH) at different plume ages during the first in-plume approach to the ship. While there is a dramatic reduction in particle number as the plume is diluted, the peak position of the number distribution changes relatively little with plume age. Middle Panel: Chemically resolved mass distribution during the first in-plume approach to the ship. The noisy distributions (right axis) correspond to measurements made after the plume had aged for ~24 min while the much smoother distributions (left axis) were obtained in the fresh plume immediately behind the ship. Again, there is little change other than a decrease in particle mass. Bottom Panel: The organic:sulfate mass ratio vs measured by the C-ToF-AMS in the ship exhaust plume.

TABLE 4. Summary of Absorption Coefficient and Nonrefractory (n.r.) Dry Particulate Composition in the Ship Exhaust Plume at Various Plume Ages

est. plume age (min)	0	24	62	out of plume
altitude (m)	30	30	55	35–220
sulfate (% n.r. dry mass)	68	67	70	73
organic mass (% n.r. dry mass)	31	31	28	18
nitrate (% n.r. dry mass)	<1	<1	<1	1
NH_4:SO_4 (mol ratio)	0.1	0.1	0.1	0.5
m/z 57:org (% n.r. dry mass)	4	3	2	0.6
m/z 44:org (% n.r dry mass)	3	5	8	17
oxalate:org (% n.r. dry mass)	1	1	2	9
org acids:org (% n.r. dry mass)	2	1	2	9
CN:SO_4 ($10^{15}g^{-1}$)	2.6	2.5	2.3	0.25
B_{ABS}:SO_4 ($Mm^{-1}g^{-1}$)[a]	2.4×10^5	2.8×10^5		

[a] Measured at 532 nm by the PSAP.

fraction can be estimated using the mass fraction of organic and inorganic species from the C-ToF-AMS, the mass fraction of water from ISORROPIA, assuming volume additivity, and assuming dry densities of 1.83 g cm^{-3} for sulfuric acid, 1.79 g cm^{-3} for ammonium bisulfate, and 1.77 g cm^{-3} for ammonium sulfate. For the purpose of calculating the organic density, all in-plume sulfate was assumed to be sulfuric acid and all out-of-plume sulfate was assumed to be in the form of ammonium sulfate. Organics were found to have a density of ~1.6 g cm^{-3} in the exhaust plume while outside of the exhaust plume there was high variability in the calculated organic density and a typical organic density of 1.4 g cm^{-3} was assumed. It is important to note that changing the organic density from 1.4 to 1.6 g cm^{-3} results in an ~1% change in predicted growth factor.

Hygroscopic growth factors of in-plume aerosol are suppressed relative to those measured in the background aerosol. In-plume aerosol has a higher fraction of organic mass (0.28 ± 0.02 vs 0.20 ± 0.15 out of plume), but also has more acidic sulfate (see Table 4). Based on measured composition and the assumptions noted above, both in- and out-of-plume hygroscopic growth factors are overpredicted by eq 1, and the overprediction within the plume is more substantial. The color bar in Figure 9 shows the hygroscopic growth factor of the organic fraction that would need to be assumed to achieve closure between the predicted and measured growth factors. While physically unrealistic, organic growth factors less than 1 indicate that observed growth factors are less than those predicted based on water uptake by the inorganic fraction alone. The presence of negative organic growth factors indicates that the measured growth factors are substantially less than predicted. Using size-resolved chemistry from the C-ToF-AMS in eq 1 would result in a slightly lower mass fraction of organics, eliminating the possibility that a high organic mass fraction was masked by averaging across particle sizes. None of the wet number distributions from the DASH-SP (74, 85, and 92% RH) shows signs of a bimodal distribution, making it improbable that an externally mixed, hydrophobic mode existed to explain the overpredicted particle hygroscopic growth factors. Potential explanations for the suppressed growth factors observed will be discussed subsequently.

3.6. CCN Activity. Figure 10 shows predicted and measured CCN concentrations for a number of points within the ship exhaust plume. These particular in-plume points were chosen because the particle concentrations were relatively stable during an entire scan of the DMA. Again, the sulfate molar ratio, SR = [NH_4^+]/[SO_4^{2-}], was used to determine the composition of the inorganic fraction (see Section 2.5). As noted earlier, the low SR suggests that the aerosol sulfate was present mostly as H_2SO_4 in the exhaust plume, while out of plume the particulate sulfate was partially neutralized. All predictions shown are based on eqs 2 and 3, but with different inputs for particulate chemical composition. Before CCN prediction calculations were performed, the dry particle size distribution was estimated based on the measured humid DMA size distribution and C-ToF-AMS measured composition as described in Section 2.5. Because the particulate composition in the ship exhaust plume did not change significantly with distance from the ship, the dry size
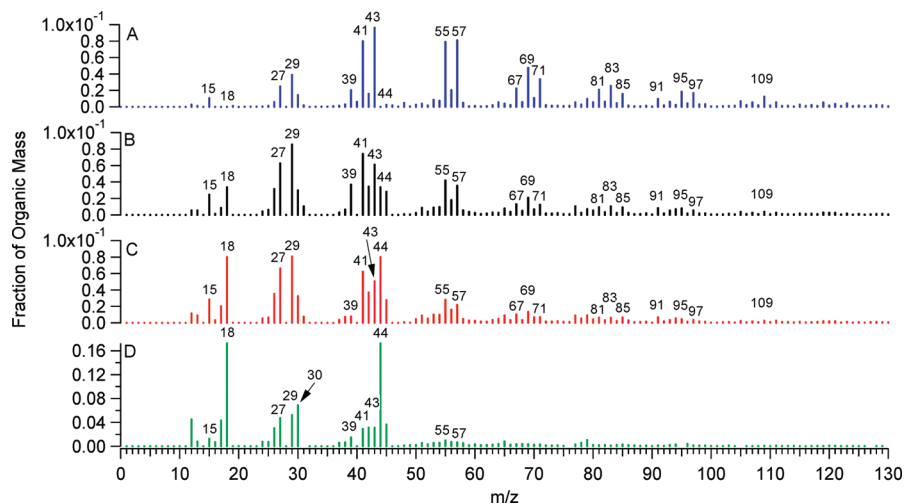
FIGURE 8. (A) Reference AMS organic mass spectrum from the diesel bus chase study of Canagaratna et al. (*48*). C-ToF-AMS organic mass spectra from (B) the ship exhaust plume a few hundred meters behind the stack, (C) the ship exhaust plume after it had aged for ~62 min, (D) background aerosol in the marine boundary layer outside of the ship exhaust plume. Signal at *m/z* 39 (typically indicative of potassium and not included in organic spectra) is shown because, based on peak location in the raw spectra (not shown), it does not appear to be potassium. Both spectra (A) and (B) strongly resemble the ship-exhaust organic AMS spectra observed by Phinney et al. (*49*).
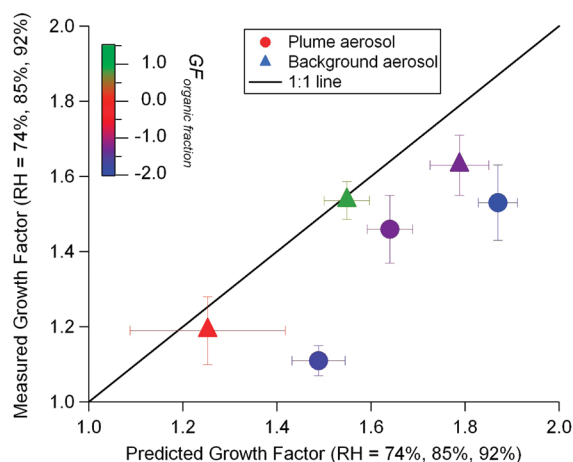

FIGURE 9. Hygroscopic growth factors for particles measured by the DASH-SP and predicted using the volume-weighted mixing rule using bulk chemical composition form the C-ToF-AMS and the assumption that organics have a growth factor of unity. Growth factors are smaller within the exhaust plume than in the background aerosol. Growth factors are suppressed relative to predictions in both the background and the plume aerosol, but the suppression is significantly more dramatic within the exhaust plume. The organic mass fraction is 0.28 ± 0.02 within the plume and 0.20 ± 0.15 outside of the plume. The color scale gives the growth factor that the organic fraction would be required to have to achieve closure between measurements and observations.
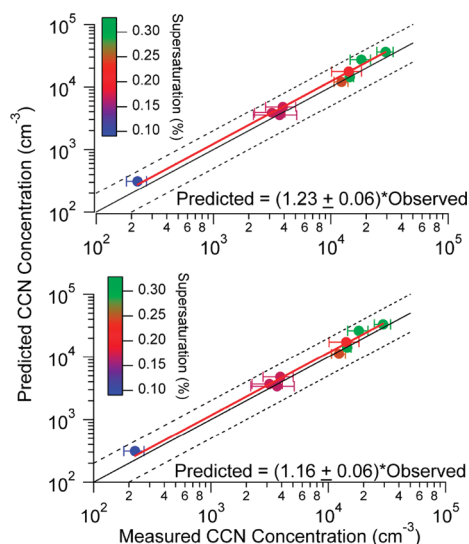

FIGURE 10. CCN droplet closure within the exhaust plume. Top Panel: Results obtained using bulk (size-averaged) chemistry. Bottom Panel: Results obtained when size-resolved chemistry is used in the calculations. Size-resolved chemistry slightly improves the closure. The color of the markers corresponds to the CCNc instrument operating supersaturation during the measurement. Dashed lines indicate values that are twice and one-half of the 1:1 line, whereas the red lines indicate the least-squares best fit. The slopes of the least-squares fits are given in the predicted vs observed equations at the bottom of each panel.

distribution was consistently between 15 and 28% smaller than the humid distributions shown in Figure 7. Organics were treated as hydrophobic (based on AMS spectra and DASH-SP results) with a density of 1.6 g cm^{-3} and were assumed to have no effect on surface tension. Assuming an internal mixture and using bulk composition results in an overprediction of CCN number by an average of 23 ± 6% (Figure 10, top). Using size-resolved composition improves the closure slightly, resulting in an average overprediction of 16 ± 6% (Figure 10, bottom). The slight improvement in closure using size resolved chemistry occurs because at the higher supersaturations (above ~0.25%) the CCN activation

diameter moves toward smaller particles, which have a higher mass fraction of hydrophobic organics and are less CCN active.

Figure 11, which will be referred to as a growth kinetics plot, shows the average diameter achieved by activated particles when exiting the CCNc growth chamber as a function of the instrument supersaturation. Because the aerosol introduced into the CCNc is polydisperse, the particles leaving the activation columns will always exhibit a range of final sizes (this occurs even if the particles are pure ammonium sulfate, because initially larger particles will grow to correspondingly larger sizes). The smallest size that an ammonium sulfate particle can reach is that attained by a particle
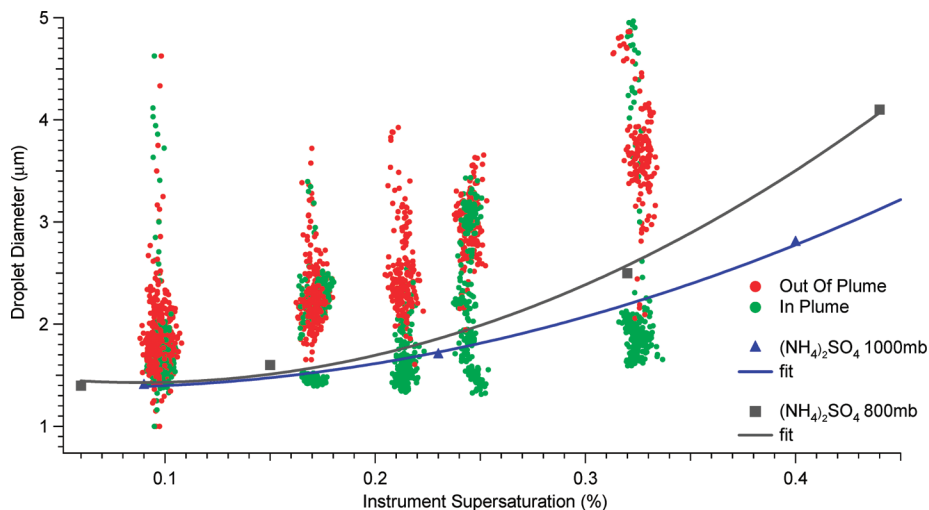
FIGURE 11. Growth kinetics plot for aerosol in and out of the ship exhaust plume. All measurements were made between 845 and 900 mbar, near the middle of the pressure range defined by the two ammonium sulfate calibrations shown in the figure. The calibration lines represent the final diameter achieved by ammonium sulfate particles with the minimum diameter required for activation at the given supersaturation. The vast majority of background particles grow to diameters greater than the minimum defined by the calibrations while the rate of growth of particles within the exhaust plume appears to be suppressed relative to that of ammonium sulfate.

of the minimum diameter required for activation at the operating supersaturation of the instrument; the lines shown in the figure represent this minimum size for ammonium sulfate particles. Any particles attaining a final size smaller than this minimum are likely be subject to mass transfer limitations; that is, water is taken up more slowly such that the particles activate at a later time within the CCNc growth chamber than ammonium sulfate. It is clear that in-plume particles tend to achieve a smaller size within the CCNc growth chamber than the reference ammonium sulfate particles. The effect is not thought to be the result of depleted supersaturation in the column which has been shown not to occur for CCN concentrations $<10^4$ cm^{-3}. This suggests that particles with critical supersaturation between 0.1 and 0.35% may have slower water uptake kinetics than ammonium sulfate. On the contrary, the vast majority of particles outside the ship plume do not exhibit slower water vapor uptake kinetics relative to $(NH_4)_2SO_4$.

4. Discussion

4.1. Comparison of Ship and Airborne Data. One goal of the present study is to determine the extent to which in-stack measurements of particulate ship emissions reflect particle properties in the airborne exhaust plume. Owing to a lack of measurements of gas-phase tracers of dispersion (e.g., CO_2 or CO), it is not possible to relate the absolute particulate mass measured in the stack to that in the air, but it is possible to assess agreement between composition measurements. In-stack particulate composition data are summarized in Table 3, while the airborne measurements are given in Table 4. The airborne measurements for sulfate are reported without associated water. Accordingly, the 6.5 H_2O molecules assumed to be associated with a sulfate molecule in the stack can be removed to give a dry sulfate emission factor of 0.84 g kWh^{-1}. To relate the shipboard and airborne organic measurements, it is necessary to estimate a conversion from organic carbon (OC), measured in the stack, to organic mass (OM) measured by the airborne C-ToF-AMS.

Aiken et al. (*47*) used a high resolution Aerodyne aerosol mass spectrometer, capable of unambiguously measuring the oxygen and carbon content of an aerosol, to relate the O:C atomic ratio to the fraction of signal intensity observed at *m/z* 44 on unit mass resolution AMS instruments. The relationship, derived from several ground-based and airborne studies, between the fraction of the organic aerosol signal (OA) present at *m/z* 44 and the atomic ratio of oxygen to carbon (O:C), given with 95% confidence intervals, is ($R^2 = 0.84$):

$$O:C = (0.0382 \pm 0.0005)(\% \text{ of OA from } m/z \, 44) + (0.0794 \pm 0.0070) \quad (4)$$

Aiken et al. (*47*) used an even broader data set, including several chamber studies in addition to the previously mentioned field studies, to derive a relationship between organic mass (OM) and the O:C atomic ratio ($R^2 = 0.997$):

$$OM/OC = (1.260 \pm 0.002)(O:C) + (1.180 \pm 0.001) \quad (5)$$

In Table 4, the percentage of the organic mass spectrum represented by signal at *m/z* 44 for particles within the exhaust plume is 3.5%, which, using eqs 4 and 5, leads to an OM:OC ratio of 1.45. The in-plume percentage of nonrefractory organic mass was measured to be 31% by the C-ToF-AMS which converts to 21% organic carbon using this estimated OM:OC ratio. Based on the arguments above, the estimated ratio of organic carbon to dry sulfate mass (OC:SO$_{4dry}$) measured in the ship's stack is 0.23 ± 0.03. The estimated airborne measurement of OM:SO$_{4dry}$ = 0.43 ± 0.01, which converts (again assuming an OM:OC ratio of 1.45) to OC:SO$_{4dry}$ = 0.30 ± 0.01. However, this relatively good agreement between airborne and shipboard measurements is a best case scenario given the previously mentioned overestimation of organic carbon mass in the shipboard measurement caused by adsorption of gas-phase organics onto the filter (estimated to be ~30% based on Shah et al. (*42*)). Because there was no correction for absorption of gas-phase organics in this study, 0.23 represents an upper limit of the organic carbon to dry sulfate mass ratio measured within the ship's stack.

There are several possible explanations for the higher fraction of organic mass measured in the airborne plume. The in-stack measurements were made at a dilution ratio of about 5:1 which is less dilute than the airborne measurements, even close to the stack. However, additional dilution should cause semivolatile organics to revolatilize and cause less organic mass to be present in the airborne plume. Loss of particulate or semivolatile gaseous organics during the transition from the stack to the filter is likely to be a negligible effect because a transfer line was not used in this study. The slightly higher temperature of the collection point for

TABLE 5. Gas and Particulate Emission Factors in g (kg fuel)$^{-1}$ from This and Previous Studies of Emissions from Ships Burning Heavy Fuel Oil

	this study	Petzold et al. 2004, 2008 (*9, 11*)	Chen et al. 2005 (*54*)	Sinha et al. 2003 (*3*)	Hobbs et al. 2000 (*7*)
NO$_x$(as NO[a])	65.7 ± 0.3[d]	112[c]	30 ± 12[e]	65.5 ± 3.3[e]	23 ± 5[e]
CO	1.5 ± 0.1[d]			3.0 ± 0.2[e]	
SO$_2$	59.7 ± 0.5[c]	51[c]	27 ± 4[e]	52.2 ± 3.7[e]	62 ± 25[e]
PM	12.9 ± 0.1[d]				
EC	0.04 ± 0.01[d]	0.18 ± 0.02[f]			
OC	0.98 ± 0.03[d], 1.3 ± 0.5[e]				
Sulfate	4.3 ± 0.5[d]				
CN 10^{16}	1.3 ± 0.2[e,g]	1.36 ± 0.24[e,g], 3.43 ± 1.26[f,g]	4.7 ± 1.3[e]	6.2 ± 0.6[e]	1.6 ± 0.5[e]
CN 10^{15}(0.1−3 μm)	0.6 ± 0.1[e]	2.3 ± 0.7[e]		5.1 ± 0.5[e]	
CCN/CN (0.3% S)	0.24 ± 0.05[e]			0.18 ± 0.07[e]	
OM:SO$_4$	0.42 ± 0.02[e]	0.54[f], 0.17[b,f]			

[a] Form of NO$_x$ not specified in Petzold et al. [b] OC:SO$_4$ ratio given in Petzold et al. (2004). [c] Calculated based on fuel composition. [d] In-stack measurement. [e] Airborne plume measurement. [f] Test-bed MAN B&W four-stroke marine diesel engine. [g] CN emissions factor reported for CN > 10 nm (reported in the current study because the 3025 CPC gave suspect results in the emissions plume).

the filters (∼25 °C) versus the ambient temperature of the marine boundary layer (14.3 ± 0.4 °C) is also judged to be relatively unimportant based on previous studies in which diesel exhaust filters were collected at different temperatures (*51*). However, it should be noted that the volatilities of the organics in the heavy fuel oil may have quite different temperature dependencies than those of organics in diesel fuels previously tested.

Given that the higher fraction of particulate organic mass observed in the airborne measurements does not appear to be an artifact of the shipboard measurement methods, the organic material must condense from the gas phase into the particle phase between the point where the stack measurements are made (at the bottom of the stack) and the point at which airborne measurements are first made (∼100 m behind the ship). Between the two measurement points, the exhaust gas from the stack passes through a heat exchanger designed to use the otherwise waste heat of exhaust (also called a waste heat boiler). The heat exchanger can lower the temperature of exhaust to ∼75−100 °C. This temperature decrease occurs without dilution of the exhaust as opposed to the dilution tunnel system used for in-stack measurements where the exhaust was cooled and diluted simultaneously. The hypothesis that organics condense in the upper regions of the stack and in the waste heat boiler is supported by Figures 3 and 7, which show that the fraction of organic mass is constant with particle size in the stack measurements but that organic mass is enriched on smaller airborne particles. This pattern of larger mass fraction on smaller particles, which have more surface area, is consistent with a gas-to-particle condensational process (assuming the condensing organic is nonvolatile enough not to be affected by the higher vapor pressure caused by the increased curvature of the smaller particles).

4.2. Plume Dilution and Aging. Because of the favorable wind and cloudless conditions during the study, it was possible to fly directly in the exhaust plume until it had reached an estimated age of 24 min and to detect the plume in transects up to an estimated age of 62 min. Measurements of plume composition at different ages are given in Table 4. Of significance is the fact that there is essentially no change in the organic:sulfate mass ratio with time. This constant ratio indicates that condensed organics in the particulate phase were not volatile enough to repartition back to the gas phase as the plume diluted and gas-phase organic concentrations decreased. Additionally, while organic matter does appear to condense into the particle phase between the lower stack (where in-stack measurements were made) and the point where airborne measurements were first made (a few hundred meters behind the ship), no further organic matter condenses into the particle phase as the plume ages after the point of the first airborne measurements.

While the ratio of organic:sulfate mass remains essentially constant, the fraction of the mass spectrum represented by the peak at m/z 44 does increase significantly with increasing plume age, indicating an increasingly oxidized aerosol. This appears to be the result of the mixing of plume and background aerosol. As shown in Figure 8 and tabulated in Table 4, the fraction of the organic signal at m/z 44 is significantly higher (17%) in the background marine aerosol than it is in the freshly emitted plume (3%). The average mass loading of organic aerosol in the background air is 0.48 μg m^{-3}, while closest to the ship it is 148 μg m^{-3}. During the transect at a plume age of 62 min, the peak organic mass loading observed was 2.0 μg m^{-3}. Accordingly, one can approximate the organic mass spectrum during this transect as a linear combination of 0.48 μg m^{-3} (24%) background aerosol and 1.52 μg m^{-3} (76%) plume aerosol. Assuming the mass spectrum of the plume aerosol remains unchanged after 62 min of aging, this simple linear combination of plume and background aerosol predicts that 6.4% of the organic signal will be present in the peak at m/z 44, which is close to the 8% that is observed. From this analysis, it appears that there is little change in the mass spectrum of the particulate organic during the first hour after emission. The conclusion that the increase in signal at m/z 44 with plume age is a result primarily of dilution lends further confidence to the hypothesis that the mass fraction and composition of particulate organics are determined soon after the exhaust is emitted from the ship.

4.3. Hygroscopic Growth. Particulate hygroscopic growth is suppressed in the ship exhaust plume relative to the background aerosol. While there is a higher fraction of organic mass inside the plume (31%) relative to the background aerosol (18%), the closure study using the volume-weighted mixing rule shows that when this organic mass is accounted for there is relatively good closure between predicted and measured growth factors outside of the exhaust plume but very poor closure within it. It is worth noting that while the closure outside the exhaust plume is reasonable, it was obtained by assuming that organics have the lowest physically realistic growth factor of unity. It is somewhat surprising that a growth factor of unity would be appropriate for the highly oxidized organics found outside of the exhaust plume, though significant mass fractions of insoluble organics and lower than predicted growth factors have been previously been observed in marine aerosols in this region (*52*).

The fact that the simple volume-weighted mixing rule with compositional inputs from C-ToF-AMS measurements is unable to realistically represent the hygroscopic behavior of the mixture of fresh, hydrocarbon-like organic and sulfuric acid found within the plume could be explained in several ways. First and most probable, the DASH-SP may not be able to fully dry the exhaust-plume particles which contain large amounts of sulfuric acid. If the particles are not fully dried before they are humidified, then the measured growth factor will be underestimated because the particle's dry size is overestimated. A second possibility is that the organic material in the exhaust plume may be slowing uptake of water onto the particles. A simple model of the DASH-SP growth chamber, which has a particle residence time of $\sim$4 s, indicates that an accommodation coefficient (α) of $\sim$10^{-4} (or equivalently slow mass transfer through the organic layer) is required to simulate the measured growth factors at 85 and 92% RH (an even smaller α ($\sim$10^{-5}) is required to simulate the measured growth factor at 74% RH, but the sizing of OPC in the DASH-SP is questionable at this lower RH because of uncertainties in the refractive index).

The final possibility is that the volume fraction of organics has been incorrectly estimated. This is possible because the particles that the DASH-SP measures (150–200 nm) are at the edge of the volume/mass distribution where there is relatively poor signal-to-noise. Figure 7 clearly shows that a 200 nm mobility diameter particle is at the tail end of the volume distribution and that the corresponding C-ToF-AMS composition measurements in this region of the mass distribution are rather uncertain. It is also important to remember that the volume distribution given in Figure 7 is given at $\sim$45% RH and would be shifted to smaller sizes (by $\sim$20%, see section 2.5) if it were dry. However, there is no obvious indication that the fraction of organics would dramatically increase at larger particle sizes and a brief sensitivity study showed that a 60% reduction in sulfate volume fraction is needed to predict the growth factors measured in the exhaust plume at 85% and 92% RH (an even further reduction of sulfate volume fraction would be needed to simulate the measurements at 74% RH). This type of reduction in sulfate seems improbable.

For completeness, it is important to note that black carbon is not detected by the C-ToF-AMS, though it is clearly present in the exhaust plume as shown by the PSAP measurements. Particles containing significant fractions of black carbon will be assigned erroneously high volume fractions of water-soluble inorganics based on C-ToF-AMS composition measurements. Despite this, the effect of black carbon is estimated to be relatively minor overall given the good agreement between C-ToF-AMS measured particle mass and DMA measured particle volume and given the low ash content in the fuel.

4.4. CCN Closure. Ship emissions are clearly a source of particles in the marine boundary layer, but because these particles typically have a smaller mean diameter and contain more organic than background marine particles, it is uncertain what fraction act as CCN under the relatively low supersaturations of marine stratocumulus clouds. The results of this study imply that, for the size distribution of particles emitted from this ship, knowledge of the size-resolved chemical composition is relatively unimportant for supersaturations below 0.3%. However, if the supersaturation is above 0.3% or if the emitted particles are slightly larger, knowledge of the size-resolved composition becomes critical for accurately predicting CCN because of the high mass fractions of hydrophobic organics, which inhibit CCN formation, observed at smaller particle sizes.

The impact of soot (black carbon) and ash particles on CCN closure was also considered. Because the C-ToF-AMS cannot detect refractory material, the presence of soot or ash will lead to overprediction of CCN. This overprediction occurs because measurements from the C-ToF-AMS are used to assign chemical compositions to the volume distribution measured by the DMA. If present, soot and ash will be measured by the DMA and assigned an incorrect composition based on the C-ToF-AMS measurements of the nonrefractory aerosol. Because soot and ash tend to be less CCN active than mixed organic/sulfate particles, this leads to an overestimation of CCN number. Based on the PSAP measurements and the estimate based on fuel composition given in Table 3, soot and ash appear to be a relatively minor contributor to aerosol mass and their presence is not expected to be a major for the overestimation of CCN number concentration, though it may partially account for the slight overestimation of CCN calculated for this study.

5. Implications

The ship studied here, with a 2-stroke, slow-speed diesel engine, represents a very common class of vessel. Emission factors from this study and relevant literature studies of ships burning heavy fuel oil are given in Table 5. All emission factors have been normalized to be in units of (kg fuel)$^{-1}$ using the carbon dioxide balance method which was also used, in slightly varying forms, in all of the previous literature cited in Table 5. This method is based on the fact that CO_2 is the principal carbon emission from combustion of HFO (while carbon is also emitted as CO, methane, nonmethane organic compounds (NMOC), and particulate mass, the mass contribution of these species is insignificant relative to CO_2). Assuming complete combustion to CO_2 and a hydrogen to carbon ratio of 1.8 for the fuel (53), 3.2 kg of CO_2 is formed per kg of fuel burned. Because CO_2 was measured in the stack, this conversion factor can be used to convert in-stack emission factors to a (kg fuel)$^{-1}$ basis. Because neither CO_2 nor other gas-phase species were measured on the airborne platform, in-plume particulate measurements were scaled to in-stack CO_2 using particulate sulfate mass measurements (made on both the shipboard and airborne platforms) and assuming that perturbations in sulfate particulate mass above background atmospheric levels were caused solely by the ship exhaust. A potential source of error in this method is that the mass of particulate sulfate could change between the stack measurements and the atmosphere; however, further conversion is unlikely.

The SO_2 emission factors in Table 5 give some confidence that the heavy fuel oil being burned in these different studies was relatively similar, at least in terms of percent sulfur. The NO_x measured in the ship's stack during this study is significantly higher than any of the previous airborne measurements. While it is similar to the Petzold et al. study (11), their numbers were estimated based on fuel composition and knowledge of engine operating conditions. While the CN emission factor varies between studies, all of the data show that the number of CN with diameters above 100 nm is roughly an order of magnitude less than the number of CN with diameters smaller than this. This study represents the second time that an emission factor for CCN has been calculated. The fraction of CN (>10 nm in diameter) that activate into CCN at 0.3% supersaturation was found to be 0.24, similar to the 0.18 found by Sinha et al. (3). Finally, the airborne organic to sulfate mass ratio from this study (which is significantly higher than the in-stack measurement) agrees well with the most recent test-bed results of Petzold et al. (11); both of these estimates are significantly higher than the previous estimate from Petzold et al. (9) which was used by Eyring et al. (1) to estimate global emissions of 0.134 Tg OC per year; these results suggest that the global annual emissions of organic carbon may be significantly higher than previously estimated.

Acknowledgments

Note Added after ASAP Publication

The Acknowledgments were modified in the version of this paper that published ASAP February 4, 2009; the corrected version published ASAP February 13, 2009.

Supporting Information Available

Information detailing the methods used for the in-stack measurements presented in this study is given in Section S1. Figure S1 gives a flow diagram of the sampling system used onboard the container ship. Figure S2 gives vertical profiles of relative humidity and potential temperature in and above the marine boundary layer. Figure S3 give 3-day NOAA Hysplit back trajectories for the air mass present during the study. This material is available free of charge via the Internet at http://pubs.acs.org.

Literature Cited

(1) Eyring, V.; Kohler, H. W.; van Aardenne, J.; Lauer, A. Emissions from international shipping: 1. The last 50 years. *J. Geophys. Res.* **2005**, *110*, D17305, doi: 10.1029/2004JD005619.

(2) Capaldo, K.; Corbett, J. J.; Kasibhatla, P.; Fischbeck, P.; Pandis, S. N. Effects of ship emissions on sulphur cycling and radiative climate forcing over the ocean. *Nature* **1999**, *400* (6746), 743–746.

(3) Sinha, P.; Hobbs, P. V.; Yokelson, R. J.; Christian, T. J.; Kirchstetter, T. W.; Bruintjes, R. Emissions of trace gases and particles from two ships in the southern Atlantic Ocean. *Atmos. Environ.* **2003**, *37* (15), 2139–2148.

(4) Corbett, J. J.; Winebrake, J. J.; Green, E. H.; Kasibhatla, P.; Eyring, V.; Lauer, A. Mortality from ship emissions: A global assessment. *Environ. Sci. Technol.* **2007**, *41*, 8512–8518.

(5) Lauer, A.; Eyring, V.; Hendricks, J.; Jockel, P.; Lohmann, U. Global model simulations of the impact of ocean-going ships on aerosols, clouds, and the radiation budget. *Atmos. Chem. Phys.* **2007**, *7*, 5061–5079.

(6) Corbett, J. J.; Koehler, H. W. Updated emissions from ocean shipping. *J. Geophys. Res.* **2003**, *108*, D20, doi: 10.1029/2003jd003751.

(7) Hobbs, P. V.; Garrett, T. J.; Ferek, R. J.; Strader, S. R.; Hegg, D. A.; Frick, G. M.; Hoppel, W. A.; Gasparovic, R. F.; Russell, L. M.; Johnson, D. W.; O'Dowd, C.; Durkee, P. A.; Nielsen, K. E.; Innis, G. Emissions from ships with respect to their effects on clouds. *J. Atmos. Sci.* **2000**, *57* (16), 2570–2590.

(8) Kasper, A.; Aufdenblatten, S.; Forss, A.; Mohr, M.; Burtscher, H. Particulate emissions from a low-speed marine diesel engine. *Aerosol Sci. Technol.* **2007**, *41* (1), 24–32.

(9) Petzold, A.; Feldpausch, P.; Fritzsche, L.; Minikin, A.; Lauer, A.; Bauer, H. Particle emissions from ship engines. In *Journal of Aerosol Science Supplement 2*, European Aerosol Conference: Budapest, 2004; *35*, S1095–S1096.

(10) Williams, E.; Lerner, B.; Quinn, P.; Bates, T. Measurements of gas and particle emissions from commercial marine vessels, AGU Fall Meeting Abstracts, 2005.

(11) Petzold, A.; Hasselbach, J.; Lauer, P.; Baumann, R.; Franke, K.; Gurk, C.; Schlager, H.; Weingartner, E. Experimental studies on particle emissions from cruising ship, their characteristic properties, transformation and atmospheric lifetime in the marine boundary layer. *Atmos. Chem. Phys.* **2008**, *8* (9), 2387–2403.

(12) Agrawal, H.; Malloy, Q. G. J.; Welch, W. A.; Miller, J. W.; Cocker, D. R. In-use gaseous and particulate matter emissions from a modern ocean going container vessel. *Atmos. Environ.* **2008**, *42* (21), 5504–5510.

(13) Agrawal, H.; Welch, W. A.; Miller, J. W.; Cocker, D. R. Emission measurements from a crude oil tanker at sea. *Environ. Sci. Technol.* **2008**, *42* (19), 7098–7103.

(14) Corbett, J. J. New directions: Designing ship emissions and impacts research to inform both science and policy. *Atmos. Environ.* **2003**, *37* (33), 4719–4721.

(15) *ISO 8178-1 Reciprocating Internal Combustion Engines - Exhaust Emission Measurement—Part 1: Test-Bed Measurement of Gaseous Particulate Exhaust Emissions*, 1st ed.; International Standards Organization: Geneva, 1996; *8*, 150.

(16) Protection of the environment. In *Code of Federal Regulations*, 40 CFR 86; U.S. Government Printing Office: Washington, DC.

(17) Shah, S. D.; Ogunyoku, T. A.; Miller, J. W.; Cocker, D. R. On-road emission rates of PAH and n-alkane compounds from heavy-duty diesel vehicles. *Environ. Sci. Technol.* **2004**, *39* (14), 5276–5284.

(18) Siegl, W. O.; Richert, J. F. O.; Jensen, T. E.; Schuetzle, D.; Swarin, S. J.; Loo, J. F.; Prostak, A.; Nagy, D.; Schlenker, A. M. Improved emissions speciation methodology for phase II of the auto/oil air quality improvement research programs hydrocarbons and oxygenates. In *SAE Technical Paper 1993, Series No. 930142, Special Publication sp-1000*; Society of Automotive Engineers: Washington, DC, 1993.

(19) *NIOSH Manual of Analytical Methods*; National Institute of Occupational Safety and Health: Cincinnati, OH, 1996.

(20) Dekati mass monitor (DMM). http://www.dekati.com/cms/dmm.

(21) Drewnick, F.; Hings, S. S.; DeCarlo, P.; Jayne, J. T.; Gonin, M.; Fuhrer, K.; Weimer, S.; Jimenez, J. L.; Demerjian, K. L.; Borrmann, S.; Worsnop, D. R. A new time-of-flight aerosol mass spectrometer (TOF-AMS) - instrument description and first field deployment. *Aerosol Sci. Technol.* **2005**, *39*, 637–658.

(22) Bahreini, R.; Dunlea, E. J.; Matthew, B. M.; Simons, C.; Docherty, K. S.; DeCarlo, P. F.; Jimenez, J. L.; Brock, C. A.; Middlebrook, A. M. Design and operation of a pressure-controlled inlet for airborne sampling with an aerodynamic aerosol lens. *Aerosol Sci. Technol.* **2008**, *42* (6), 465–471.

(23) Huffman, J. A.; Jayne, J. T.; Drewnick, F.; Aiken, A. C.; Onasch, T.; Worsnop, D. R.; Jimenez, J. L. Design, modeling, optimization, and experimental tests of a particle beam width probe for the aerodyne aerosol mass spectrometer. *Aerosol Sci. Technol.* **2005**, *39*, 1143–1163.

(24) Canagaratna, M. R.; Jayne, J. T.; Jimenez, J. L.; Allan, J. D.; Alfarra, M. R.; Zhang, Q.; Onasch, T. B.; Drewnick, F.; Coe, H.; Middlebrook, A.; Delia, A.; Williams, L. R.; Trimborn, A. M.; Northway, M. J.; DeCarlo, P. F.; Kolb, C. E.; Davidovits, P.; Worsnop, D. R. Chemical and microphysical characterization of ambient aerosols with the aerodyne aerosol mass spectrometer. *Mass Spectrom. Rev.* **2007**, *26* (2), 185–222.

(25) Sorooshian, A.; Brechtel, F. J.; Ma, Y. L.; Weber, R. J.; Corless, A.; Flagan, R. C.; Seinfeld, J. H. Modeling and characterization of a particle-into-liquid sampler (PILS). *Aerosol Sci. Technol.* **2006**, *40* (6), 396–409.

(26) Sorooshian A. NgN. L. ChanA. W. H. FeingoldG. FlaganR. C. SeinfeldJ. H. Particulate organic acids and overall water-soluble aerosol composition measurements from the 2006 Gulf of Mexico Atmospheric Composition and Climate Study (Go-MACCS) *J. Geophys. Res.* **2007**, *112*, D13, D13201, doi: 10.1029/2007JD008537.

(27) Virkkula, A.; Ahlquist, N. C.; Covert, D. S.; Arnott, W. P.; Sheridan, P. J.; Quinn, P. K.; Coffman, D. J. Modification, calibration and a field test of an instrument for measuring light absorption by particles. *Aerosol Sci. Technol.* **2005**, *39* (1), 68–83.

(28) Sorooshian, A.; Hersey, S.; Brechtel, F. J.; Corless, A.; Flagan, R. C.; Seinfeld, J. H. Rapid, size-resolved aerosol hygroscopic growth measurements: Differential aerosol sizing and hygroscopicity spectrometer probe (DASH-SP). *Aerosol Sci. Technol.* **2008**, *42* (6), 445–464.

(29) Roberts, G. C.; Nenes, A. A continuous-flow streamwise thermal-gradient CCN chamber for atmospheric measurements. *Aerosol Sci. Technol.* **2005**, *39* (3), 206–221.

(30) Lance, S.; Medina, J.; Smith, J. N.; Nenes, A. Mapping the operation of the DMT continuous flow CCN counter. *Aerosol Sci. Technol.* **2006**, *40* (4), 242–254.

(31) Aklilu, Y.; Mozurkewich, M.; Prenni, A. J.; Kreldenweis, S. M.; Alfarra, M. R.; Allan, J. D.; Anlauf, K.; Brook, J.; Leaitch, W. R.; Sharma, S.; Boudries, H.; Worsnop, D. R. Hygroscopicity of particles at two rural, urban influenced sites during pacific 2001: Comparison with estimates of water uptake from particle composition. *Atmos. Environ.* **2006**, *40*, 2650–2661.

(32) Gysel, M.; Crosier, J.; Topping, D. O.; Whitehead, J. D.; Bower, K. N.; Cubison, M. J.; Williams, P. I.; Flynn, M. J.; McFiggans, G. B.; Coe, H. Closure study between chemical composition and hygroscopic growth of aerosol particles during TORCH2. *Atmos. Chem. Phys.* **2007**, *7* (24), 6131–6144.

(33) Seinfeld, J. H.; Pandis, S. N., *Atmospheric Chemistry and Physics: From Air Pollution to Climate Change*, 2nd ed.; Wiley-Interscience: Hoboken, N. J., 2006.

(34) Clegg, S. L.; Brimblecombe, P.; Wexler, A. S. Thermodynamic model of the system $H^+-NH_4^+-Na^+-SO_4^{2-}-NO_3^--Cl^--H_2O$ at 298.15 K. *J. Phys. Chem. A* **1998**, *102* (12), 2155–2171.

(35) Wexler, A. S.; Clegg, S. L.; Brimblecombe, P. On-line aerosol inorganics model. http://mae.ucdavis.edu/~sclegg/aim.html.

(36) Medina, J.; Nenes, A.; Sotiropoulou, R. E. P.; Cottrell, L. D.; Ziemba, L. D.; Beckman, P. J.; Griffin, R. J. Cloud condensation nuclei closure during the International Consortium for Atmospheric Research on Transport and Transformation 2004 campaign: Effects of size-resolved composition. *J. Geophys. Res.* **2007**, D10S31, doi: 10.1029/2006jd007588.

(37) Nenes, A.; Pandis, S. N.; Pilinis, C. Isorropia: A new thermodynamic equilibrium model for multiphase multicomponent inorganic aerosols *Aquat. Geochem.* **1998**, *4*123152, http://nenes.eas.gatech.edu/ISORROPIA.

(38) Brechtel, F. J.; Kreidenweis, S. M. Predicting particle critical supersaturation from hygroscopic growth measurements in the humidified TDMA. Part I: Theory and sensitivity studies. *J. Atmos. Sci.* **2000**, *57* (12), 1854–1871.

(39) Brechtel, F. J.; Kreidenweis, S. M. Predicting particle critical supersaturation from hygroscopic growth measurements in the humidified TDMA. Part II: Laboratory and ambient studies. *J. Atmos. Sci.* **2000**, *57* (12), 1872–1887.

(40) Rose, D.; Gunthe, S. S.; Mikhailov, E.; Frank, G. P.; Dusek, U.; Andreae, M. O.; Poschl, U. Calibration and measurement uncertainties of a continuous-flow cloud condensation nuclei counter (DMT-CCNC): CCN activation of ammonium sulfate and sodium chloride aerosol particles in theory and experiment. *Atmos. Chem. Phys.* **2008**, *8* (5), 1153–1179.

(41) Draxler, R. R.; Rolph, G. D. Hysplit (hybrid single-particle lagrangian integrated trajectory) model access via NOAA ARL ready website. http://www.arl.noaa.gov/ready/hysplit4.html.

(42) Shah, S. D.; Cocker, D. R.; Miller, J. W.; Norbeck, J. M. Emission rates of particulate matter and elemental and organic carbon from in-use diesel engines. *Environ. Sci. Technol.* **2004**, *38* (9), 2544–2550.

(43) DeCarlo, P. F.; Slowik, J. G.; Worsnop, D. R.; Davidovits, P.; Jimenez, J. L. Particle morphology and density characterization by combined mobility and aerodynamic diameter measurements. Part 1: Theory. *Aerosol Sci. Technol.* **2004**, *38* (12), 1185–1205.

(44) Zhang, Q.; Alfarra, M. R.; Worsnop, D. R.; Allan, J. D.; Coe, H.; Canagaratna, M. R.; Jimenez, J. L. Deconvolution and quantification of hydrocarbon-like and oxygenated organic aerosols based on aerosol mass spectrometry. *Environ. Sci. Technol.* **2005**, *39*, 4938–4952.

(45) Kondo, Y.; Miyazaki, Y.; Takegawa, N.; Miyakawa, T.; Weber, R. J.; Jimenez, J. L.; Zhang, Q.; Worsnop, D. R. Oxygenated and water-soluble organic aerosols in Tokyo. *J. Geophys. Res* **2007**, *112*, doi: 10.1029/2006jd007056.

(46) Takegawa, N.; Miyakawa, T.; Kawamura, K.; Kondo, Y. Contribution of selected dicarboxylic and omega-oxocarboxylic acids in ambient aerosol to the m/z 44 signal of an Aerodyne aerosol mass spectrometer. *Aerosol Sci. Technol.* **2007**, *41*, 418–437.

(47) Aiken, A. C.; DeCarlo, P. F.; Kroll, J. H.; Worsnop, D. R.; Huffman, J. A.; Docherty, K.; Ulbrich, I. M.; Mohr, C.; Kimmel, J. R.; Sueper, D.; Zhang, Q.; Sun, Y.; Trimborn, A.; Northway, M.; Ziemann, P. J.; Canagaratna, M. R.; Onasch, T. B.; Alfarra, R.; Prevot, A. S. H.; Dommen, J.; Duplissy, J.; Metzger, A.; Baltensperger, U.; Jimenez, J. L. O/C and OM/OC ratios of primary, secondary, and ambient organic aerosols with high resolution time-of-flight aerosol mass spectrometry. *Environ. Sci. Technol.* **2008**, *42* (12), 4478–4485.

(48) Canagaratna, M. R.; Jayne, J. T.; Ghertner, D. A.; Herndon, S.; Shi, Q.; Jimenez, J. L.; Silva, P. J.; Williams, P.; Lanni, T.; Drewnick, F.; Demerjian, K. L.; Kolb, C. E.; Worsnop, D. R. Chase studies of particulate emissions from in-use New York City vehicles. *Aerosol Sci. Technol.* **2004**, *38* (6), 555–573.

(49) Phinney, L.; Leaitch, W. R.; Lohmann, U.; Boudries, H.; Worsnop, D. R.; Jayne, J. T.; Toom-Sauntry, D.; Wadleigh, M.; Sharma, S.; Shantz, N. Characterization of the aerosol over the sub-arctic north east Pacific Ocean. *Deep-Sea Res. Part II* **2006**, *53* (20−22), 2410–2433.

(50) McLafferty, F. W.; Turecek, F., *Interpretation of mass spectra*, 4th ed.; University Science Books: Sausalito, CA, 1993; p 371.

(51) Cocker, D. R.; Shah, S. D.; Johnson, K. C.; Zhu, X. N.; Miller, J. W.; Norbeck, J. M. Development and application of a mobile laboratory for measuring emissions from diesel engines. 2. Sampling for toxics and particulate matter. *Environ. Sci. Technol.* **2004**, *38* (24), 6809–6816.

(52) Kaku, K. C.; Hegg, D. A.; Covert, D. S.; Santarpia, J. L.; Jonsson, H.; Buzorius, G.; Collins, D. R. Organics in the northeastern pacific and their impacts on aerosol hygroscopicity in the subsaturated and supersaturated regimes. *Atmos. Chem. Phys.* **2006**, *6*, 4101–4115.

(53) Tuttle, K. L. Combustion-generated emissions in marine propulsion systems. In *Environmental Symposium: Ship Design and Operation in Harmony with the Environment*; Society of Naval Architects and Marine Engineers: Jersey City, NJ, 1995; pp 311−323.

(54) Chen, G.; Huey, L. G.; Trainer, M.; Nicks, D.; Corbett, J.; Ryerson, T.; Parrish, D.; Neuman, J. A.; Nowak, J.; Tanner, D.; Holloway, J.; Brock, C.; Crawford, J.; Olson, J. R.; Sullivan, A.; Weber, R.; Schauffler, S.; Donnelly, S.; Atlas, E.; Roberts, J.; Flocke, F.; Hubler, G.; Fehsenfeld, F. An investigation of the chemistry of ship emission plumes during ITCT 2002. *J. Geophys. Res.* **2005**, *110*, D10.

ES802413J